Genomics of Root System Architecture Adaptation in Sorghum under Nitrogen and Phosphorus Deficiency

Joshua Magu[1], Joel Masanga[2], Catherine Muui[3], Steven Runo[1*]

[1]Department of Biochemistry, Microbiology and Biotechnology, Kenyatta University, P O Box 43844-00100, Nairobi, Kenya

[2]Department of Biology, The Pennsylvania State University, 432 Science Drive, University Park, PA 16802, USA

[3]Department of Agricultural Science and Technology, Kenyatta University, P O Box 43844-00100, Nairobi, Kenya

Corresponding author email: runo.steve@ku.ac.ke

Key words

Genome wide association study (GWAS), Nitrogen deficiency, Phosphorus deficiency, Root System Architecture

Abstract

Plant root systems play a crucial role in water and nutrient uptake so understanding the genetic mechanisms underlying root architecture adaptation to the environment is key, particularly in non-model crops. Here, we investigate the diversity of root system architecture (RSA) in *Sorghum bicolor* under nitrogen (N) and phosphorus (P) deficiency. We used a globally diverse sorghum panel to identify single nucleotide polymorphisms (SNPs) associated RSA responses under N and P deficiency through a genome-wide association study (GWAS). RSA adaptation under P deficiency involved development of fine exploratory roots marked by increased total root length and fine root classes (root length diameter ranges 1 and2), coupled with reduced radial expansion. Under N deficiency, adaptation also involved suppression of root radial growth

but without elongation. In both cases, reduced radial growth was marked by reduced surface area and volume, more dramatically for P than N deficiency. GWAS identified SNPs associated with these RSA adaptations, some of which were in regions encoding genes such as: *ILR3-like*, *bHLH*, and a *LEUNIG* homolog all with known roles in root growth regulation. These findings provide novel genetic insights into sorghum root adaptation to nutrient limitations and offer potential targets for breeding resource-efficient crop varieties.

Summary

Plants absorb water and nutrients from the soil through their roots, yet for most crops, little is known about how root shape and structure adapt to stressful conditions such as poor soil fertility. In this study, we used a globally diverse collection of sorghum genotypes to investigate how sorghum roots respond to nitrogen and phosphorus deficiency. Specific genotypes showed strong root adaptations under these conditions, leading us to identify genetic factors significantly associated with these responses. Our findings improve our understanding of root adaptation to nutrient stress and highlight promising genetic targets for breeding more nutrient-efficient crops.

Introduction

Sorghum (*Sorghum bicolor* L. Moench) is a globally important cereal crop used for food, feed, and bioenergy. It can survive adverse conditions such as high temperatures and drought (Trouche et al. 2014), making it a strategic crop for mitigating the impacts of climate change. However, sorghum production in many regions is constrained by poor soil fertility (Khalifa and Eltahir 2023). Specifically, nitrogen (N) and phosphorus (P) are critical determinants of yield (White and Brown 2010); yet their availability is often limited due to depleted soils and the high cost or limited accessibility of fertilizers (Sheahan and Barrett 2017). One way to address nutrient limitations is to exploit plants' natural ability to adapt their root system architecture (RSA) to optimize nutrient extraction in resource-limited environments.

53 Previous studies (Parra-Londono et al. 2018) have described three major rooting system
54 types: (i) a small root system, (ii) a compact and bushy root system, and (iii) an exploratory root
55 system, each conferring potential adaptive advantages under nutrient-limited conditions.
56 Genotypes with compact, bushy, and shallow root systems are thought to be better adapted to
57 P scarcity while those with exploratory root systems may be better suited to N scarcity (Parra-
58 Londono et al. 2018). This diversity in RSA underlies strong genotype-dependent responses to
59 nutrient stress. For example, under low P conditions, specific sorghum genotypes respond by
60 increasing root length (Parra-Londono et al. 2018). To offset the metabolic constraints imposed
61 by P deficiency, such plants have reduced secondary growth, resulting in longer, thinner roots
62 (Strock et al. 2017).
63 Given the importance of these adaptations, this study aimed to identify RSA changes in
64 sorghum under N and P deficiency, as well as the genetic regions that underpin these traits for
65 possible integration into breeding programs targeting nutrient-limited ecosystems.
66 We hypothesized that sorghum genotypes exhibit extensive genetic variation for RSA
67 traits, based on the species' ecological adaptations. To test this hypothesis, we used 123
68 accessions of the sorghum reference set, representing all major cultivated, wild, and
69 intermediate sorghum races from diverse agroecological regions across Africa, India, the Middle
70 East, Europe, and North America (Casa et al. 2008). This panel which comprises mainly
71 landraces, but also contain wild genotypes, breeding material, and advanced cultivars has
72 proven effective for identifying new traits, including parasitic plants (*Striga*) resistance (Kavuluko
73 et al. 2021).
74 Numerous technologies are now available for root imaging and phenotyping, including
75 hydroponic root elutriation systems (Box et al. 1989), minirhizotron and coring methods (Box et
76 al. 1989; Phillips et al. 2000), non-destructive radar and electrical resistance tomography (Ducut
77 et al. 2022), and root crown phenotyping (Seethepalli et al. 2020). In this study, we used a
78 modified root crown phenotyping approach involving excavation of the upper root system,

removal of the growth substrate (vermiculite), and subsequent measurements. The integrated RhizoVision Crown platform (Seethepalli et al. 2020) provided a reliable way to extract data from numerous root systems. Similar platforms have been successfully used in studies of nutrient acquisition in crops such as soybean (*Glycine max*), common bean (*Phaseolus vulgaris*), cowpea (*Vigna unguiculata*), wheat (*Triticum aestivum*), and maize (York 2018).

With advances in high-throughput RNA sequencing (RNA-seq), quantitative trait loci (QTL) can now be resolved at the gene level. In our study, we used genotyping-by-sequencing (GBS) SNP data from the sorghum diversity panel (Morris et al. 2013). This approach has been similarly applied in sorghum (Gelli et al. 2014) to identify genes and novel transcripts involved in RSA control.

To achieve our objective of identifying genetic factors in sorghum that influence root architecture under nutrient-limited conditions, we controlled N and P availability in the growth medium and analyzed the resulting RSA changes, followed by association mapping of these traits with genotype data. We describe these findings and their implications for breeding sorghum varieties better adapted to low-nutrient environments.

Materials and Methods

Plant material

A subset comprising 123 accessions of the sorghum reference set [Dataset S1 and (https://genebank.icrisat.org/Common/Viewer?ctg=Referenceset&ref=RS1)] was obtained from the International Crops Research Institute for the Semi-Arid Tropics (ICRISAT) Nairobi, Kenya and maintained at the Plant Transformation Laboratory (Kenyatta University, Nairobi, Kenya).

Genetic description of sorghum accessions

Sorghum distribution maps were generated using MapTool package (Lemmond, 1994) in R version 4.3.1 based on metadata available at https://www.morrislab.org/data (Lasky et al. 2015).

105 To perform population genetic structure analysis, we retrieved SNP data from the repository of
106 Colorado State University (Morris et al. 2013), available at https://www.morrislab.org/data.
107 Population genetic structure was analyzed using phylogenetic and Bayesian clustering
108 methods.

109 For phylogenetic analysis, we first converted the retrieved SNP HapMap file into Variant
110 Call Format (VCF) using TASSEL (Trait Analysis by aSSociation, Evolution and Linkage)
111 version 5.0 (Bradbury et al. 2007). The resulting VCF file was then utilized to construct a
112 neighbor-joining (NJ) tree with the 'ape' package (Paradis et al. 2004) in R.

113 For Bayesian clustering, the SNP HapMap file was transformed into PLINK format using
114 TASSEL, then ADMIXTURE software employed to analyze population clusters, evaluating K
115 values ranging from 1 to 10. The optimal number of clusters was determined based on the K
116 value with the lowest cross-validation error. The ADMIXTURE results were visualized using
117 plots generated with the ggplot2 package (Villanueva and Chen 2019) in R.

118 SNP density was calculated in 50 kb windows using genomic positions extracted from
119 PLINK binary files. Marker quality was assessed based on minor allele frequency and per-
120 marker missing genotype rate. Linkage disequilibrium (LD) was estimated as pairwise r^2 for SNP
121 pairs within the same chromosome and up to 500 kb apart. And LD decay analyzed by binning
122 SNP pairs into 10 kb intervals and computing the mean r^2 per bin for each chromosome and
123 plots were generated using ggplot2 (Villanueva and Chen 2019).

124

125 **Sorghum seedling establishment**

126 Sorghum seedlings were sowed in pots measuring 13.5 cm × 11 cm × 11 cm containing
127 vermiculite. For each of the 123 sorghum accessions, 5 seedlings were selected and planted in
128 3 replicates (5 seedlings per pot in controlled complete randomized) and 3 treatments of
129 watering with; Long Ashton media (Hudson 1967) (optimal N and P), Long Ashton media minus
130 N, and Long Ashton Media minus P. Pots were laid out in a complete randomized block and

131 maintained in the greenhouse for 14 days. Greenhouse conditions were set and maintained at a
132 light/ dark cycle of 12/12 h and a temperature of 28℃ day and 24℃ nights.
133
134 **Root imaging and analysis of sorghum phenotypes**
135 On the 14th day, fresh root samples were photographed using a Nikon DX VR 18–140 mm
136 camera at a resolution of 1400 dpi. The acquired images were processed and analyzed using
137 RhizoVision Explorer, (https://www.rhizovision.com/) an open-source software designed for root
138 phenotyping.
139 Images were firstly scaled and cropped to produce grayscale versions, followed by the
140 application of a global image threshold to distinguish roots (foreground) from the background
141 using the software's 'Broken Roots' mode. The pixel-to-centimeter conversion was calibrated to
142 41.02 pixels per mm. Image thresholding was set to 150 to achieve clear root boundaries while
143 minimizing external noise. Non-root artifacts smaller than 2 mm^2 were filtered out to prevent
144 interference with the analysis. Edge smoothing was enabled and set to level 2 to reduce false
145 root appearances during skeletonization, thereby enhancing the delineation of root features.
146 The root pruning threshold was configured to remove false root segments where tips are shorter
147 than the diameter of the primary root, ensuring accurate feature extraction. RhizoVision Explorer
148 output 13 RSA traits, were exported as .csv files (Dataset S2).
149
150 **Data analysis**
151 RhizoVision data (Dataset S2) were used for downstream analysis in R version 4.3.1.
152 Hierarchical clustering was performed using the agnes() function from the cluster package
153 (Maechler et al. 2026) using Ward's method and clusters visualized using dendrograms. PCA
154 was performed on all RSA traits using the FactoMineR package (Lê et al. 2008) and biplots
155 generated with the factoextra package (Kassambara and Mundt 2020). Correlation analyses
156 were performed using the corrplot package (Wei and Simko 2021), and additional statistical

analysis with the PerformanceAnalytics package (Peterson 2020). Gaussian graphical models (Glasso networks) were generated using the qgraph package (Epskamp et al. 2012). Node centrality measures were calculated from the Glasso networks using the centrality() function. Linear mixed-effects models were performed using the lme4 package (Bates et al. 2015) and Forest plots generated using ggplot2.

Analysis of variance was performed to evaluate the effect of genotype; effect of environment; and effect of both genotype and environment on root traits. Mean separation was performed using Tukey's Honest Significant Difference (HSD) test at $p \leq 0.05$. Heritability of each trait under the tree conditions was estimated according to (Hill et al. 2008)

$$h^2 = \frac{\sigma_G^2}{\sigma_G^2 + \sigma_{G\times E}^2 \frac{1}{n} + \sigma^2 \frac{1}{n \times r}}$$

Where σ_G^2 represent the genotypic variance, $\sigma_{G\times E}^2$ denotes variance of genotype by environment interaction, σ^2 error of variance, n number of environments and r number of replicates.

Genome wide association studies (GWAS)

Genome-wide association studies (GWAS) were conducted on RSA phenotypes under three conditions: optimal, nitrogen-deficient, and phosphorus-deficient. A total of 264,962 previously developed and filtered single nucleotide polymorphisms (SNPs) (Morris et al. 2013) were used for genome-wide association analysis. GWAS was first conducted on individual RSA traits under each treatment condition, followed by analysis of traits that showed significant associations in a multivariate framework. All analyses were performed using the Genome Association and Prediction Integrated Tool (GAPIT) version 2 (Tang et al. 2016), implementing three models: Bayesian-information and Linkage-disequilibrium Iteratively Nested Keyway (BLINK) (Huang et al. 2018) , the Fixed and Random Model Circulating Probability Unification (FarmCPU) (Kusmec and Schnable 2018) and the Multi-Locus Mixed Model (MLMM) (Segura et al. 2012). To correct for multiple testing, we applied a 5% false discovery rate (FDR). The results were visualized

using quantile-quantile (QQ) plots and Manhattan plots. Significant SNPs associated with the phenotypic traits were mapped onto the *Sorghum bicolor* genome using Phytozome v3.1.1's JBrowse tool (Goodstein et al. 2012). Candidate genes of interest were selected based on their proximity to the SNPs and their potential involvement in the regulation of root development.

Results

Description of sorghum root system architecture

To extract root data from various sorghum genotypes, we used the RhizoVision platform, which provided 13 root traits. These traits are illustrated in Figure 1 and described in more detail in Table S1. The traits can be grouped as follows: (i) Size: Total root length (TRL), Perimeter (P), Surface Area (SA), Network Area (NA), and Volume (V); (ii) Extent: Branch Points (BP), Branching Frequency (BF), and Number of Root Tips (NRT); (iii) Distribution: Average diameter (AD), Median diameter (MD), and Maximum diameter (MD).

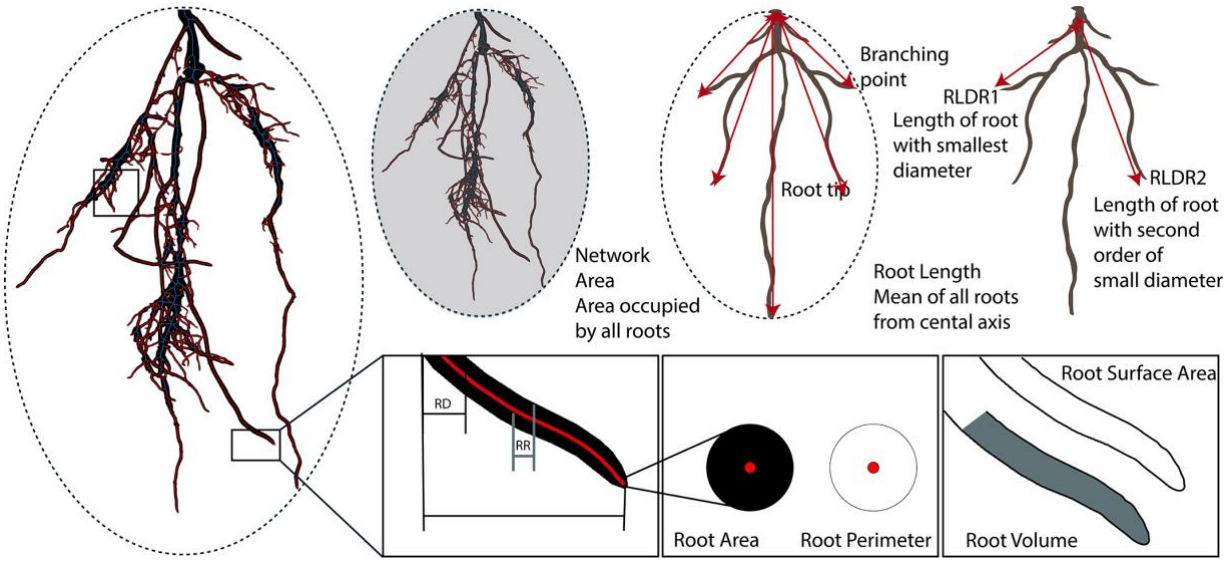

Figure 1. RhizoVision analysis of root system architecture showing a skeletonized sorghum root image used to extract measurements. The upper panel shows measurement for network area (left panel), root length, root tip and branching point (middle panel) and root length diameter range 1 (RLDR1) and RLDR2 (right panel). The lower panel shows a small root region that is amplified to show root diameter (RD), and root radius (RR) in the left panel, root area and root perimeter (middle panel) and root volume and root surface area (right panel). Scale of skeletonized root crown = 140 mm.

195

196 **Genetic variation of sorghum root system architecture and response to N and P nutrients**
197 **deficiency**

198 To examine genetic variation in the sorghum root system we used a subset of 123 genotypes of
199 the sorghum diversity panel (Figure S1a). The panel was highly diverse and comprised all major
200 sorghum races. Phylogenetic analysis using Neighbor-Joining grouped the genotypes into major
201 clades corresponding to races: bicolor, caudatum, durra, guinea, Guinea subraces, kafir and
202 wild genotypes with some clusters showing admixture (Figure S1b). These same groupings
203 were reflected in Bayesian hierarchical clustering (BHC) (Figure S1c) at the most optimal K
204 (K=4 to K=6). Plots from BHC also showed weak population structuring rather than strictly
205 discrete genetic groups. Additionally, the sorghum genotypes represented populations
206 originating in diverse agro-ecological regions across Africa, Asia, America and Europe (Billot et
207 al. 2013).

208 We then grouped the 123 genotypes used in the study based on Euclidean distances of
209 all their RSA traits. Under optimum nutrient conditions, this grouping produced 5 clusters (Figure
210 2) but under N and P deficiency, the clusters reduced to 2 suggesting that nutrient deficiency led
211 to changes on the RSA of genotypes leading to reorganized the relationships.

212

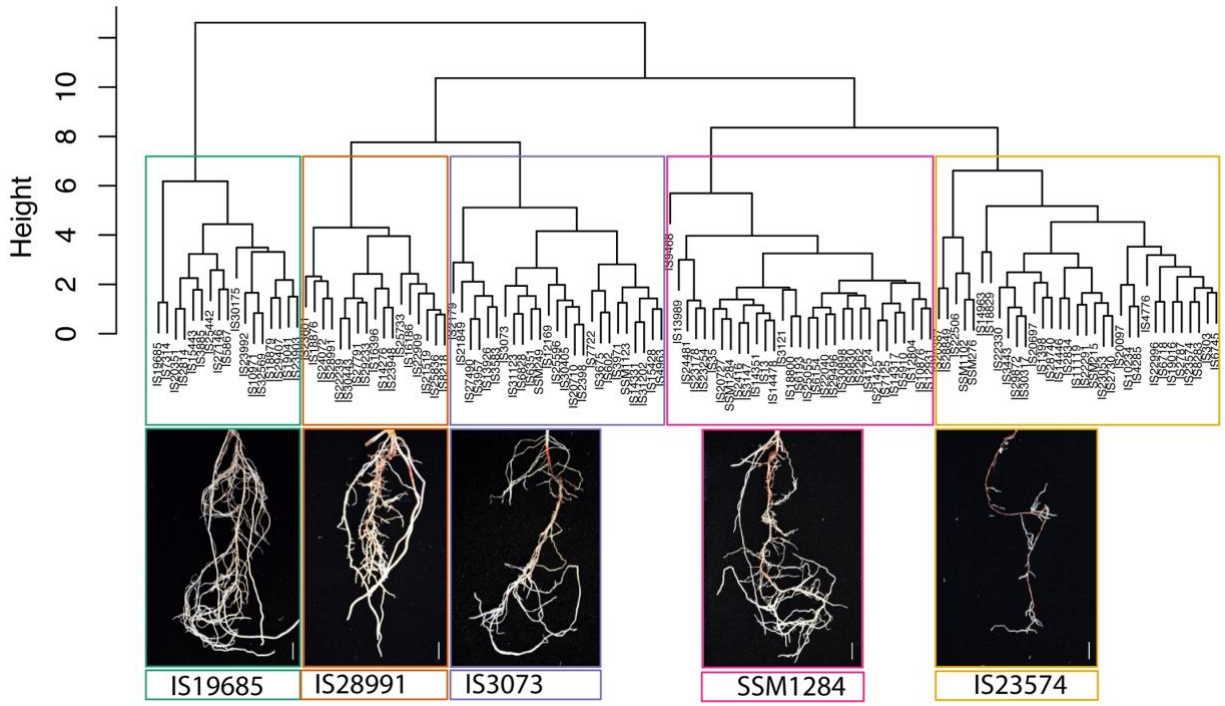

Figure 2. Variation of sorghum root architecture: Dendrogram showing clustering of root traits from a dataset of 123 sorghum genotypes. Clustering was performed using the complete method and Euclidean distance using all analyzed root system architecture traits. The colored boxes highlight five distinct root-type clusters, each represented with crown images corresponding to the genotypes within the cluster.

Partitioning of genotypic variation of sorghum root system architecture

Next, we examined how variation in RSA was partitioned among genotypes using principal component analysis (PCA) under optimal, minus N, and minus P conditions.

Under optimal nutrient conditions (Figure 3A), the first principal component (PC1; 56.9% of the variance) was mainly associated with total root length, number of root tips, number of branching points, perimeter, surface area, and root length diameter ranges 1 and 2. These traits exhibited long vectors with high contribution and loading values, indicating a strong influence on PC1 (Dataset S4). The second principal component (PC2; 31.5%) was contributed by root diameter traits: maximum diameter, average diameter, and median diameter, which were oriented oppositely to branching frequency implying negative correlation between root thickness and branching frequency.

225 Under N deficiency (Figure 3B), PC1 accounted for 62.6% of the variance contributed by
226 total root length, number of root tips, number of branch points, perimeter and root length
227 diameter ranges 1 and 2. PC2 accounting for 28.0% variance was still associated with diameter-
228 related traits, and branching frequency was also negatively aligned with PC2 like in optimal
229 conditions. RSA vectors were also notably tighter implying that they work as a module.
230 Under P deficiency (Figure 3C), PC1 explained 58.1% of the variance and remained
231 associated with total root length, number of root tips, number of branch points, perimeter and
232 root length diameter ranges 1 and 2; however, vector alignment among these traits was weaker
233 than under N deficiency. Linke in N deficiency, branching frequency contributed negatively
234 along PC2 under P deficiency.
235 Together, these patterns indicate that nutrient deficiency enhances adaptive changes in
236 RSA, with diameter (thickness) traits becoming increasingly uncorrelated from elongation and
237 branching traits under both N and P deficient conditions.
238 Analysis of individual genotypes (dots) on the PCA plots revealed that under optimal
239 conditions, genotypes were widely dispersed, reflecting high internal diversity with respect to all
240 RSAs (Figure 3A). Under N and P deficiency (Figure 3B and C) some genotypes spread
241 primarily along PC1, projecting strongly towards elongation/branching traits, and fewer towards
242 PC2 (diameter and branching frequency RSA) plausibly reflecting adaptability of these
243 genotypes based on the RSAs that they aligned with. However a majority of genotypes were at
244 the center of the PCA, suggesting that RSA traits of these genotypes do not adapt to N or P
245 deficiency.

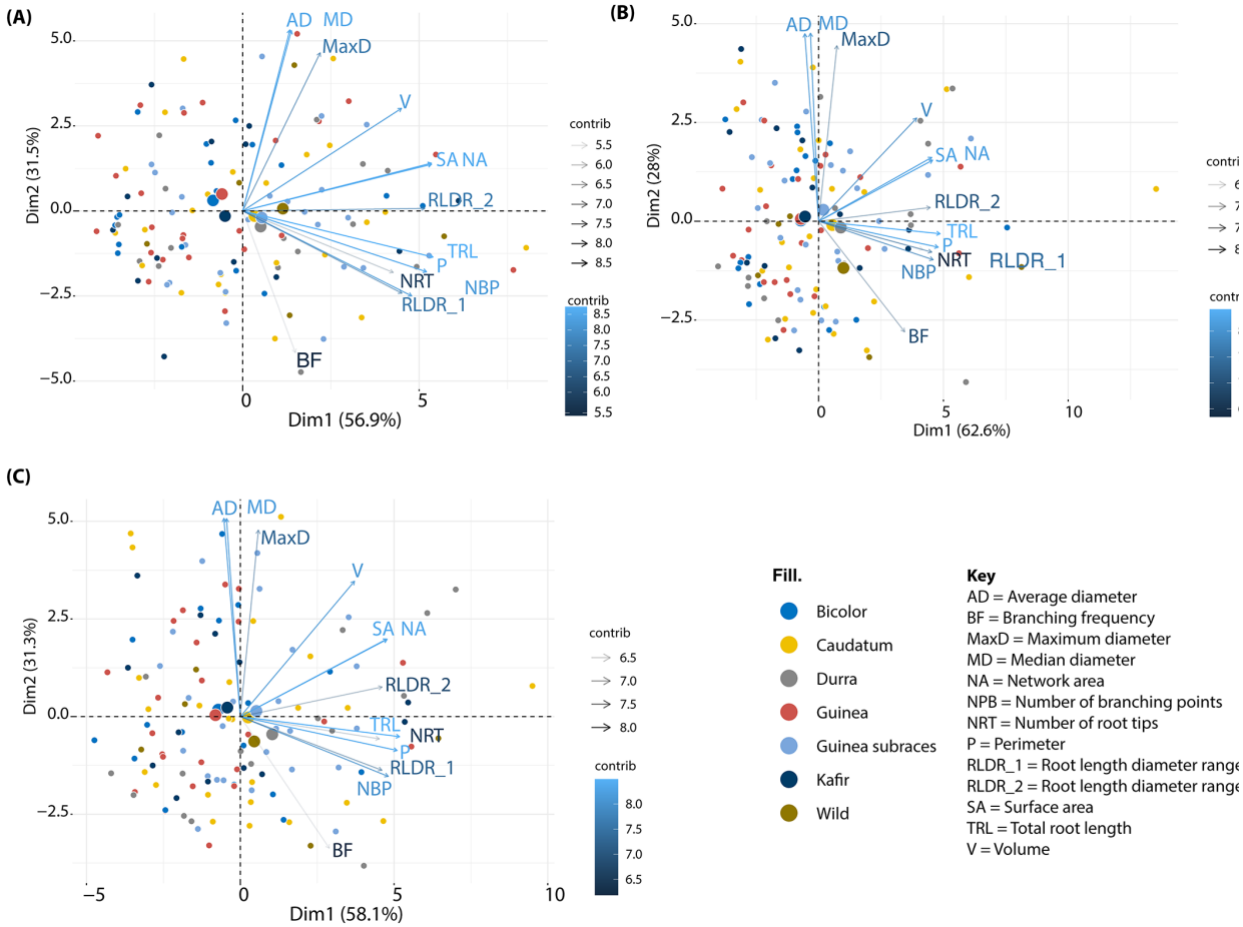

Figure 3. Principal component analysis (PCA) of root system architecture (RSA) traits across nutrient conditions. (A) optimal nutrient conditions, (B) nitrogen deficiency, and (C) phosphorus deficiency. Arrows indicate RSA trait loadings, with arrow length and color intensity reflecting the relative contribution of each trait to the principal components. Dots represent individual genotypes positioned according to their RSA trait profiles. Genotypes projecting in the direction of a given trait arrow exhibit higher values for that trait, whereas genotypes positioned opposite the arrow show lower values. The percentage of variance explained by each principal component is indicated on the axes.

Interactions of sorghum root system architecture traits

To determine levels of correlations among various RSA traits under all experimental conditions, we performed a Person's correlation analysis.

Under optimal conditions, (Figure 4A), analysis revealed that total root length was the central trait showing a strong positive correlation with all RSA traits (r > 0.77) except diameter based traits (non-significant), branching frequency (weak correlation r = 0.38) and root volume

(moderate correlation, r = 0.63). In contrast, diameter-related traits; maximum diameter, average diameter, and median diameter were negatively correlated with branching frequency.

Under N deficiency (Figure 4B), total root length showed strong positive correlations (r > 0.7) with all measured RSA traits, except for root diameter traits (maximum, average, and median diameter). Notably, these diameter-related traits exhibited negative correlations with branching frequency.

Under minus P conditions (Figure 4C), root length diameter range 2 was the central trait, showing strong positive associations with most RSA traits (r > 0.7), but no significant correlations with diameter-based traits. Its associations with branching frequency (r = 0.36) and with root length–diameter range 1 (r = 0.57) were weak. Diameter-based traits under low P conditions were more strongly and negatively correlated with branching frequency than under optimal or N-deficient conditions; for example, median diameter showed a stronger negative correlation under low P (r = −0.63) compared with optimal (r = −0.59) and low N conditions (r = −0.60).

These findings indicate that the negative association between root thickness (diameter-based RSA) and branching was consistent across treatments but strongest under P deficiency, highlighting nutrient-specific adaptations of root system architecture and plausible trade-offs between branching and thickness.

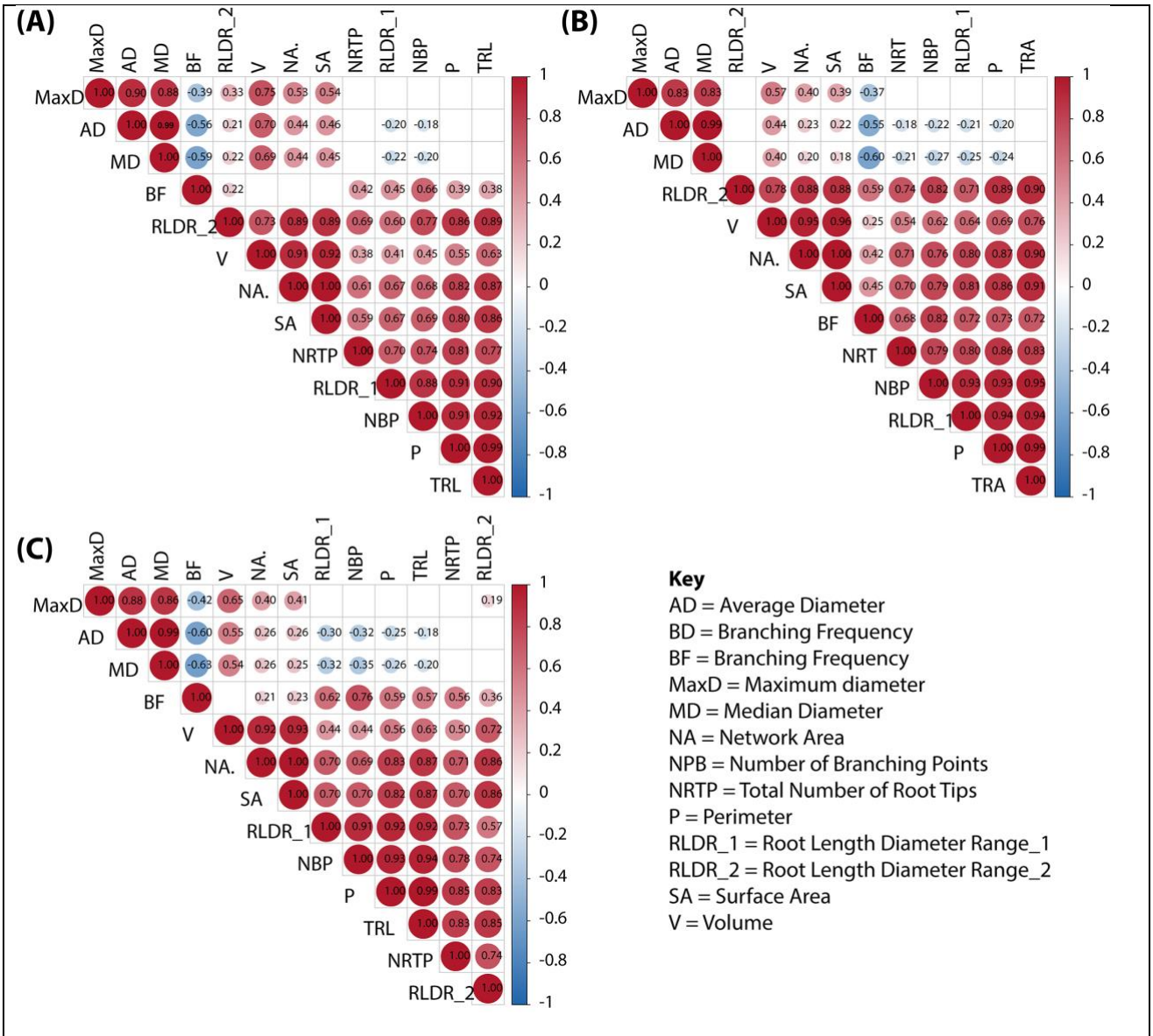

Figure 4. Pearson's correlation analysis of root system architecture traits under (A) optimal, (B) nitrogen deficiency, and (C) phosphorus deficiency conditions. Colored cells show Pearson correlation coefficients (*r*), with values displayed. Only significant correlations ($P < 0.05$) are shown, and traits are ordered by hierarchical clustering. Traits measured are shown on the key.

Gaussian graphical models (Bhushan et al. 2019) were then used to quantify conditional dependencies among root traits (Figure 5 A-C). Under optimal conditions (Figure 5A), the network was highly integrated, with strong positive partial correlations among total root length, perimeter, network area, surface area, and volume. Diameter traits formed a distinct module

that remained connected to overall root size, while branching traits were positively associated with total root length.

Under N deficiency (Figure 5B), traits clustered into modules, with total root length emerging as a central hub linking branching traits (number of branch points and branching frequency) and root length–diameter range ranges 1 and 2. There was also notable negative correlations involving diameter traits.

Under P deficiency, the network exhibited reduced connectivity, characterized by strong connectivity between total root length and root length diameter ranges 1 and 2. There were also notable negative correlations involving size and diameter traits.

These patterns indicate a shift from coordinated general root growth under optimal conditions to increasingly specialized root system architectural strategies: branched roots under N deficiency, and elongated fine roots under P deficiency with diameter traits acting negatively to the traits.

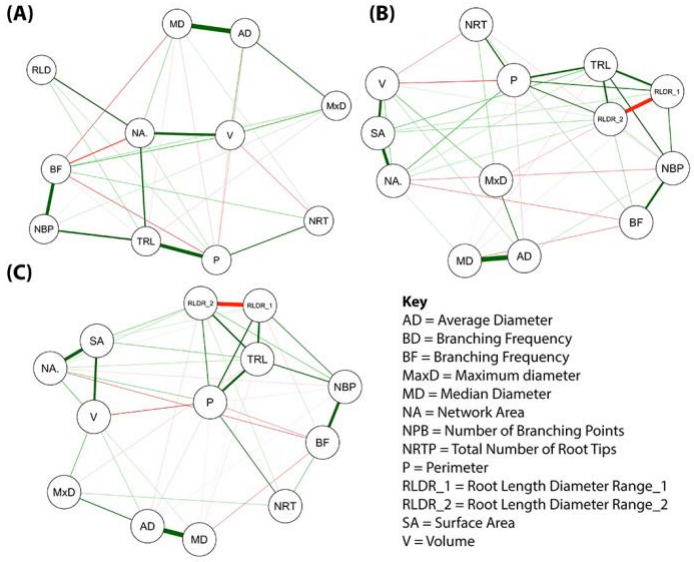

Figure 5. Gaussian graphical model showing strength of correlation between traits: A. Optimal nutrients, B, nitrogen deficiency and C. Phosphorus deficiency. Red and green lines show negative and positive correlations, respectively.

Impact of nutrient stress on sorghum root architecture

To assess the response RSA traits to N and P deficiency, we performed fixed-effects model analyses for all traits, using the optimal nutrient treatment as the reference. The results showed that root length–related traits: root length in diameter ranges 1 and 2 and total root length increased markedly under P deficiency. In contrast, RSA traits associated with secondary growth, surface area and volume, were reduced under both N and P deficiency, with a more notable reduction observed under P deficiency (Figure 6; Dataset S3).

Together, these findings indicate that P deficiency promotes an increase in total root length, largely driven by the proliferation of fine roots. This response occurs alongside a reduction in overall root surface area and volume traits under both nutrient limitations, particularly under P deficiency. In all cases, radial growth is suppressed.

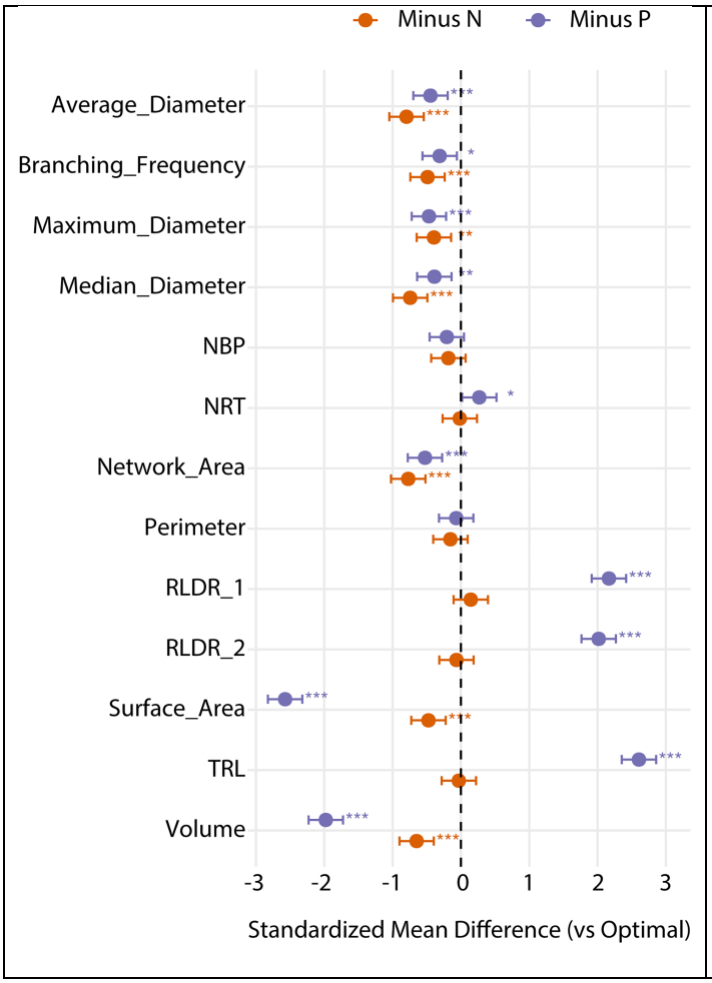

Figure 6. Impact of nutrient stress on sorghum root system architecture. Forest plot showing standardized mean differences (SMD ± 95% confidence intervals) of root system architecture traits under nitrogen and phosphorus deficiency relative to the optimal nutrient treatment (reference = 0). Positive SMD values indicate an increase relative to the optimal treatment, whereas negative values indicate a decrease.

Genome wide association studies to identify genetic factors underpinning root system architecture traits in sorghum

To investigate the genetic factors contributing to the observed RSA responses under N and P stress, we conducted GWAS on all 13 measured traits using GBS based SNP markers. Assessment of markers for this dataset SNP markers showed that they were evenly distributed across the genome with no large gaps (Figure S4). Marker quality metrics indicated low missing rates and balanced minor allele frequencies across chromosomes (Figure S4). And Linkage disequilibrium decayed within the first 100 kb and approached background levels by ~300–500 kb, (Figure S4).

317 In total, GWAS detected 25 significant SNPs detected under N and P deficiency using
318 RSA traits of volume, surface area, root length diameter range 2, and number of branching
319 points (N deficiency) and root length diameter range 2 (P deficiency).
320 The most prominent SNP was S1_26205071 identified 11 times using volume, surface
321 area, number of branching points, and root length diameter range 2, under N deficiency and root
322 length diameter range 2, under P deficiency. This SNP did not fall on a gene region, but its
323 highly significant P value and association with multiple traits in two models pointed to its
324 importance in shaping the root architecture. Therefore, we characterized the phenotypic
325 variation related to each haplotype of the SNP change. We determined that 92 and 8
326 accessions harbored the C and T haplotypes, respectively, whereas the remaining 37
327 accessions lacked genotype information. Under all environments, the accessions carrying the T
328 allele showed significantly higher values of the RSA traits surface area, root length diameter
329 range 2, and number of branching points than those carrying the C allele ($p \leq 0.05$), indicating
330 that the T haplotype had a positive effect on RSA (Figure 5C).
331 Our analysis further identified several SNPs located on annotated genes with functions
332 and phenotypes directly linked to RSA. For instance, S7_2952840 (p = 6.96E-08) was mapped
333 to a gene annotated as *ILR3-like*. *ILR3* (also known as *bHLH105*) encodes a basic helix-loop-
334 helix (bHLH) transcription factor involved in iron homeostasis (Tissot et al. 2019) putatively
335 though auxin signaling (Rampey et al. 2006). Likewise, S10_11497177 (p = 3.08E-08) was
336 found upstream of the *bHLH18*; is associated with stress response and hormone signaling
337 pathways, including ethylene and gibberellins (Cui et al. 2018). Additionally, SNP 54899232 (p =
338 8.77E-09) was positioned in the exon of a gene annotated as a transcription corepressor of
339 *LEUNIG*. Prior studies have shown that the *LEUNIG_HOMOLOG* (*LUH*) plays a critical role in
340 root elongation (Sitaraman et al. 2008).

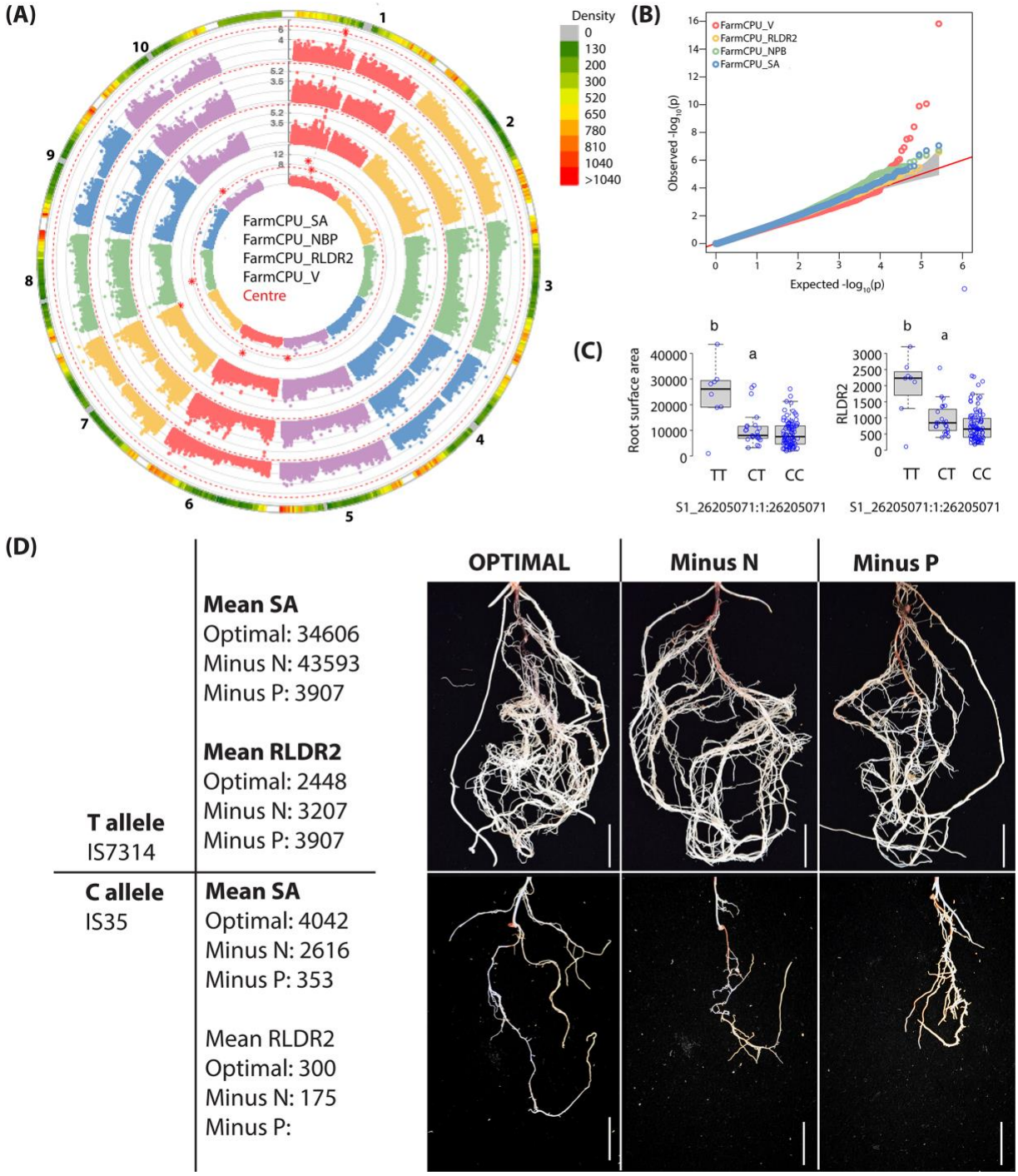

Figure 7: Genome-wide association studies identifying genetic factors influencing root system architecture traits in sorghum. (A) Fixed and Random Model Circulating Probability Unification model circular Manhattan plot highlighting significant single nucleotide polymorphisms (SNP) associated with root system architecture traits, including volume, root length diameter 2, number of branch points, and surface area. (B) Corresponding Quantile-quantile (QQ) plot comparing observed and expected p-values to assess model accuracy and false positives. (C) Boxplot illustrating the allelic effect of the most significant SNP (S1_26205071) on surface area and root length diameter range 2. Favorable alleles increase

trait expression, while unfavorable alleles decrease it. (D) Representative root phenotypes comparing "C" and "T" allele genotypes under optimal, nitrogen-deficient, and phosphorus-deficient conditions. Genotypes with the "C" allele exhibited significantly higher SA and RLD2. Scale bar = 140 mm.

Table 1. Sorghum single nucleotide polymorphisms (SNPs) showing significant genome-wide associations with root system architecture (RSA) traits (FDR correction at ∝0.05). SNPs within genes are presented with their annotations in order of chromosomal location. AF: allele frequency; AdjP: P-value after FDR adjustment. *Represent SNPs identified under nitrogen deficiency, †represent SNPs identified under phosphorus deficiency. Letters after SNP positions represent GWAS model used: a = BLINK, b = FarmCPU, c = MLMM.

Chr	Position	AF	AdjP	Associated Trait	Gene ID	Annotation
1	26205071*c	0.16	6.18E-08	Surface area	N/A	N/A
1	26205071*c	0.16	1.67E-07	Volume	N/A	N/A
1	26205071*b	0.16	4.05E-08	Surface area	N/A	N/A
1	26205071†c	0.16	1.89E-13	RLDL2	N/A	N/A
1	26205071*c	0.16	5.43E-08	Surface area	N/A	N/A
1	26205071*c	0.16	5.43E-08	Surface area	N/A	N/A
1	26205071*c	0.16	1.42E-09	RLDL2	N/A	N/A
1	26423820*c	0.20	1.05E-07	Volume	N/A	N/A
1	26731398*c	0.13	1.78E-07	Surface area	N/A	N/A
1	26731398*c	0.13	1.72E-08	Volume	N/A	N/A
1	26731398*b	0.13	1.19E-07	Surface area	N/A	N/A
1	26731398*b	0.13	3.70E-11	Volume	N/A	N/A
1	26731398*c	0.13	3.29E-08	Volume	N/A	N/A
1	27129528*c	0.10	2.20E-08	Volume	XM_002464586.2	CCRP 4 homolog
1	26205071*a	0.16	1.10E-10	Surface area	N/A	N/A
1	26423820*a	0.20	4.68E-08	Volume	N/A	N/A
1	26205071*a	0.16	1.56E-12	RLDL2	N/A	N/A
1	20102651*b	0.40	8.66E-11	Volume	N/A	N/A
2	63695738†c	0.42	2.03E-08	RLDL2	N/A	N/A
2	63695779†b	0.41	5.28E-09	RLDL2	N/A	N/A
3	15123886*b	0.10	1.97E-08	RLDL2	XP_002455526	Uncharacterized protein
3	54899232†c	0.08	8.77E-09	RLDL2	XP_02131268.1	*LEUNIG*
3	67879725*a	0.12	6.48E-11	Volume	XP_002456657.1	Cell Division Control Protein 6

4	12760823[†b]	0.28	6.82E-11	RLDL2	N/A	N/A
	5702394[*b]	0.09	8.74E-08	NBP	XP_002451690.2	Uncharacterized protein
4	58775820[*b]	0.16	3.12E-09	NBP	XP_021314639.1	*MAPK14-like*
5	17754110*b	0.04	3.38E-08	NBP	XP_002449381.2	1-aminocyclopropane-1-carboxylate oxidase 1
5	59062428[*b]	0.12	2.63E-08	Volume	N/A	N/A
6	55153514[†b]	0.08	6.48E-08	RLDL2	XP_021318054.1	E3 ubiquitin-protein ligase RNF14
6	56342501[*c]	0.03	2.55E-08	N NBP	XP_021318339.1	probable LRR receptor-like serine/threonine-protein kinase/hypothetical protein
6	56929524[*b]	0.03	4.41E-09	Volume	SORBI_3006G223101	Hypothetical protein
6	4077580[*a]	0.05	1.16E-09	NBP	XP_021318130.1	Uncharacterized protein
6	45806791[*b]	0.27	1.29E-10	Volume	XP_002446521.1	Transcription factor bHLH18
7	2952840[*c]	0.07	6.96E-08	NBP	XP_0213120712.1	ILR3
7	64170934[*b]	0.43	3.75E-13	Volume	N/A	N/A
8	15675606[*b]	0.05	3.96E-09	Volume	N/A	N/A
9	49587358[†b]	0.35	1.35E-11	NBP	N/A	N/A
9	49587358[*a]	0.35	1.44E-09	NBP	N/A	N/A
10	9879684[*b]	0.16	5.00E-09	NBP	XP_002438177.2	peroxygenase 4
10	17059423[*a]	0.35	2.99E-09	Volume	N/A	N/A
10	11497177[*b]	0.46	3.08E-08	Volume	N/A	N/A

Discussion

Sorghum exhibit variation that adapts to nitrogen and phosphorus deficiency

Root system architecture traits varied significantly among the genotypes. A HC dendrogram based on all RSA analyzed grouped the genotypes into five clusters. However, when N and P were removed, only two clusters emerged. This reduction in the number of clusters could be indicative of differences in root architecture driven by N and P deprivation as previously

356 described (Parra-Londono et al. 2018) whereby RSA types were described as: small; compact
357 and; exploratory root system, all linked to adaptation under N, P or water stress.
358
359 **Sorghum adapts to Nitrogen and Phosphorus deficiency using a root elongation-**
360 **thickness trade-off strategy**
361 PCA, pairwise correlation and Gaussian graphical models and fixed-effects model analyses all
362 showed RSA responded in a nutrient-specific manner.
363 In PCA analysis, increase in the contribution of PC1 from 56.9% under optimal
364 conditions to 62.6% under N deficiency implies that RSA contributing to the variance under N
365 deficiency (mainly root elongation and number of branch points) increased. Conversely,
366 decrease in the variance in PC2 to 28.0% indicates that the RSA in PC2 (diameter traits)
367 decreased (root elongation-thickness trade-off). This trade-off was more pronounced under P
368 deficiency as displayed by the perpendicular orientation to PC1 to diameter traits in PC2.
369 Correlation analysis and Gaussian graphical models further highlighting RSA
370 reorganization in a nutrient deficient manner with N removal showing a coordinated modular
371 organization of RSA with the total root length as the hub with negative correlations to diameter
372 measurements. P removal led to a similar switch in RSA but with root length diameter range 2
373 becoming the central trait and a more pronounced root elongation-thickness trade off – with root
374 elongation being driven by fine root classes (root length diameter ranges 1 and 2).
375 Fixed-effects model analyses affirmed root elongation-thickness trade-off whereby
376 surface area and volume, declined under both N and P deficiency, with the strongest reductions
377 observed under P limitation.
378 A similar trade-off was reported described by York et al., (2013). The authors argue that
379 thicker roots (higher root diameter) tend to be less branched or have lower branching frequency,
380 particularly in resource-constrained environments. In our study, we propose that under P
381 deficiency, sorghum reallocates growth toward elongation and proliferation of fine roots, thereby

382 increasing total root length and enhancing soil exploration capacity. Fine roots are metabolically
383 less costly to produce and provide greater absorptive surface per unit biomass, making them
384 advantageous for acquiring immobile nutrients such as phosphorus.

385 Fine root proliferation under P deficiency is consistent with results obtained in rice
386 (Wissuwa 2003; Shimizu et al. 2004; Yi et al. 2005) and in maize (Mollier and Pellerin 1999); but
387 in contrast to shorter root growth observed in Arabidopsis grown in low P conditions. The
388 varying effects of P deficiency on root development may be attributed to species and genotypic
389 variations, as Reviewed in (Niu et al. 2013). Reduced root secondary growth is consistent with
390 the notion that reduced root secondary growth decreases maintenance and construction costs,
391 allowing greater root elongation and soil exploration, thereby improving P acquisition and plant
392 growth under nutrient stress. The hypothesis was advanced by (Strock et al. 2017). Further
393 support comes from studies of sorghum RSA (Parra-Londono et al. 2018), where increased
394 elongation of lateral roots under P deficiency produced a more highly branched root system.
395

396 **GWAS reveal genetic factors associated with root system adaptation under nitrogen and**
397 **phosphorus deficiency**

398 Our GWAS analysis approach leveraging BLINK, FarmCPU and MLMM approaches
399 proved powerful in identifying SNPs associated with RSA adaptation under N and P deficiency.
400 We chose these approaches because compared to traditional single-locus mixed linear models
401 (MLM), these multi-locus models offer greater statistical power and improved resolution for
402 dissecting complex traits, increasing the likelihood of identifying associations that might
403 otherwise go undetected. FarmCPU achieves this by iteratively separating marker testing from
404 kinship correction, treating significant markers as fixed effects while modeling random
405 background variation, thus reducing false positives (Liu et al. 2016). And, MLMM extends MLM
406 by incorporating significant markers stepwise as cofactors, allowing simultaneous modeling of
407 multiple loci and capturing more complex genetic architectures (Segura et al. 2012).

408 Expectedly, SNPs were detected based on the surface area, volume, root length
409 diameter range 2 and to a lesser extent branching frequency RSAs. GWAS results revealed a
410 significant SNP that colocalized with surface area and root length diameter range 2. Further
411 analysis of phenotypic variation linked to the different haplotypes of S1_26205071 (C allele vs.
412 T allele) demonstrated the phenotypic impact of this SNP where C Allele accessions exhibited
413 significantly higher values of surface area and root length diameter range 2 . The haplotype
414 analysis confirms that this SNP is not just statistically significant but biologically relevant in
415 shaping important root traits, making it a strong candidate for further validation and
416 incorporation into breeding strategies aimed at improving root system architecture. Although no
417 gene was associated with the SNP, this SNP could be linked to a causative variant in the
418 vicinity, functioning through linkage disequilibrium. Additional fine-mapping or functional studies,
419 such as transcriptome analysis, could reveal specific genes affected by this SNP.
420 Our GWAS analysis revealed significant associations with additional SNPs located in
421 gene-coding regions, with three noteworthy genes identified: (i) The *ILR3-like* gene belongs to
422 the basic helix-loop-helix (*bHLH*) family of transcription factors, which are involved in iron
423 homeostasis, nutrient acquisition, and root development. In *Arabidopsis thaliana*, the *ILR3* gene
424 regulates iron deficiency responses in roots, which can indirectly influence root growth traits
425 under iron-limiting conditions (Tissot et al. 2019). Given its involvement in iron regulation, *ILR3-*
426 *like* may mediate crosstalk between nitrogen signaling and other nutrients, such as iron. Under
427 conditions of nutrient imbalance, such as nitrogen deficiency, *ILR3-like* might trigger structural
428 changes in roots, enhancing branching and improving nutrient foraging efficiency. (ii) *bHLH18*,
429 another member of the bHLH transcription factor family, is associated with diverse plant growth
430 and developmental processes (Cui et al. 2018) , including root development, stress responses,
431 and hormonal signaling pathways (e.g., auxin and gibberellin). The association between
432 *bHLH18* and root volume suggests that this gene may influence root growth by regulating cell
433 proliferation, expansion, or overall biomass accumulation in roots. (iii) Transcriptional Repressor

434 of *LEUNIG* (*LUH*) likely acts as a positive regulator of root elongation, influencing cell division
435 and expansion processes in the root meristem or elongation zone (Sitaraman et al. 2008). This
436 hypothesis is further supported by the identification of a SNP linked to LUH using root length
437 diameter range 2 (RLDR2) as a trait, suggesting its role in promoting elongation under specific
438 root system adaptations.

439 The associations of these genes with RSA traits suggest they may function in the same
440 or complementary pathways that modulate root structure and function. Further functional
441 genetics validation will provide critical insights into their roles and interactions, offering new
442 avenues for understanding and improving root system adaptations to nutrient stress.

443 In conclusion, our study underscores the vast genetic diversity within the sorghum gene
444 pool, making it a valuable resource for identifying alleles for germplasm improvement.
445 Integrating high-throughput root architecture phenotyping with freely accessible genomic data
446 enabled us to pinpoint genetic regions associated with RSA adaptation under nutrient-limiting
447 conditions and to infer, plausibly the biological processes involved. This knowledge may inform
448 crop breeding strategies designed to improve resilience to challenges associated with soil
449 nutrient deficiency.

450

451 **Author contributions**

452 SR and second author JM conceived and designed the study. First author JM performed the
453 experiments and all analysis guided by SR and CM. SR, and first author JM, wrote the
454 manuscript. All authors read and approved the final manuscript.

455

456 **Data availability statement**

457 The data that support the findings were derived from the following resources available in the
458 public domain: [https://www.morrislab.org/data and
459 https://genebank.icrisat.org/Common/Viewer?ctg=Referenceset&ref=RS1]. The data that

460 supports the findings of this study are available in the supplementary material of this article.
461 Dataset S1 contain the sorghum accessions metadata and Dataset S2 contain the root system
462 architecture (RSA). Data of sorghum accessions used in the study. Full results from the GWAS,
463 heritability estimates, PCA analysis, and all associated scripts used in the study have been
464 uploaded to the Genetics Society of America's Figshare portal.
465
466 **Acknowledgements**
467 This work was funded by the National Research Fund grant to S.R. contract number
468 KU/DVCR/NRF/VOL1/27 under the Multi Disciplinary Research Grants. The authors thank and
469 acknowledge the International Crops Research Institute for the Semi-Arid Tropics (ICRISAT)
470 through Dr. Eric Manyasa for availing the sorghum germplasm used in this project.
471
472
473

474 **Supplemental information**

475 The following Supporting Information is available for this article:

476 **Table S1**: Description of root system architecture (RSA) traits extracted from RhizoVision
477 analysis.

478 **Table S2.** Genetic and environmental effects on sorghum root system architecture.

479 **Figure S1.** Genetic diversity of sorghum accessions used for sorghum root system architecture
480 analysis.

481 **Figure S2.** Sorghum root clusters generated under different nitrogen and phosphorus
482 deficiency.

483 **Figure S3.** Pairwise scatterplot matrix of sorghum root system architecture.

484 **Figure S4:** Genome-wide marker distribution, quality assessment, and linkage disequilibrium
485 decay

486 **Figure S5.** Multivariate detection of Single Nucleotide Polymorphisms (SNPs) associated with
487 Root System Architecture (RSA) using multiple traits and models

488 **Dataset S1.** Sorghum accessions metadata.

489 **Dataset S2.** Root system architecture data of sorghum accessions used in the study.

490 **Dataset S3.** PCA loading and variance contributions of sorghum root system architecture

491 **Dataset S4.** Table of fixed effects and model summary of sorghum root system architecture

492

493

494

495 **References**

496 Bates D, Mächler M, Bolker B, Walker S. 2015. Fitting Linear Mixed-Effects Models Using lme4.
497 J Stat Softw. 67(1). https://doi.org/10.18637/jss.v067.i01

498 Bhushan N et al. 2019. Using a Gaussian Graphical Model to Explore Relationships Between
499 Items and Variables in Environmental Psychology Research. Front Psychol. 10:1050.
500 https://doi.org/10.3389/fpsyg.2019.01050

501 Billot C et al. 2013. Massive Sorghum Collection Genotyped with SSR Markers to Enhance Use
502 of Global Genetic Resources Yan W, editor. Plos One. 8(4):e59714.
503 https://doi.org/10.1371/journal.pone.0059714

504 Box JE, Smucker AJM, Ritchie JT. 1989. Minirhizotron Installation Techniques for Investigating
505 Root Responses to Drought and Oxygen Stresses. Soil Sci Soc Am J. 53(1):115–118.
506 https://doi.org/10.2136/sssaj1989.03615995005300010021x

507 Bradbury PJ et al. 2007. TASSEL: software for association mapping of complex traits in diverse
508 samples. Bioinformatics. 23(19):2633–2635. https://doi.org/10.1093/bioinformatics/btm308

509 Casa AM et al. 2008. Community Resources and Strategies for Association Mapping in
510 Sorghum. Crop Sci. 48(1):30–40. https://doi.org/10.2135/cropsci2007.02.0080

511 Cui Y et al. 2018. Four IVa bHLH Transcription Factors Are Novel Interactors of FIT and
512 Mediate JA Inhibition of Iron Uptake in Arabidopsis. Mol Plant. 11(9):1166–1183.
513 https://doi.org/10.1016/j.molp.2018.06.005

514 Ducut JD et al. 2022. A Review of Electrical Resistivity Tomography Applications in
515 Underground Imaging and Object Detection. Displays. 73:102208.
516 https://doi.org/10.1016/j.displa.2022.102208

517 Epskamp S et al. 2012. qgraph : Network Visualizations of Relationships in Psychometric Data.
518 J Stat Softw. 48(4). https://doi.org/10.18637/jss.v048.i04

519 Gelli M et al. 2014. Identification of differentially expressed genes between sorghum genotypes
520 with contrasting nitrogen stress tolerance by genome-wide transcriptional profiling. BMC
521 Genom. 15(1):179. https://doi.org/10.1186/1471-2164-15-179
522 Goodstein DM et al. 2012. Phytozome: a comparative platform for green plant genomics.
523 Nucleic Acids Res. 40(Database issue):D1178–D1186. https://doi.org/10.1093/nar/gkr944
524 Hill WG, Goddard ME, Visscher PM. 2008. Data and Theory Point to Mainly Additive Genetic
525 Variance for Complex Traits. PLoS Genet. 4(2):e1000008.
526 https://doi.org/10.1371/journal.pgen.1000008
527 Huang M et al. 2018. BLINK: a package for the next level of genome-wide association studies
528 with both individuals and markers in the millions. GigaScience. 8(2):giy154.
529 https://doi.org/10.1093/gigascience/giy154
530 Hudson JP. 1967. Sand and Water Culture Methods Used in the Study of Plant Nutrition. 104--
531 104
532 Kassambara A, Mundt F. 2020. Factoextra: Extract and Visualize the Results of Multivariate
533 Data Analyses. R Package Version 1.0.7. https://CRAN.R-project.org/package=factoextra
534 Kavuluko J et al. 2021. GWAS provides biological insights into mechanisms of the parasitic
535 plant (Striga) resistance in sorghum. BMC Plant Biol. 21(1):392. https://doi.org/10.1186/s12870-
536 021-03155-7
537 Khalifa M, Eltahir EAB. 2023. Assessment of global sorghum production, tolerance, and climate
538 risk. Front Sustain Food Syst. 7:1184373. https://doi.org/10.3389/fsufs.2023.1184373
539 Kusmec A, Schnable PS. 2018. FarmCPUpp: Efficient large-scale genomewide association
540 studies. Plant Direct. 2(4):e00053. https://doi.org/10.1002/pld3.53
541 Lasky JR et al. 2015. Genome-environment associations in sorghum landraces predict adaptive
542 traits. Sci Adv. 1(6):e1400218. https://doi.org/10.1126/sciadv.1400218
543 Lê S, Josse J, Husson F. 2008. FactoMineR : An R Package for Multivariate Analysis. J Stat
544 Softw. 25(1). https://doi.org/10.18637/jss.v025.i01

545 Liu X et al. 2016. Iterative Usage of Fixed and Random Effect Models for Powerful and Efficient
546 Genome-Wide Association Studies Listgarten J, editor. Plos Genet. 12(2):e1005767.
547 https://doi.org/10.1371/journal.pgen.1005767
548 Maechler M et al. 2026. cluster: Cluster Analysis Basics and Extensions. R package version
549 2.1.8.2. https://CRAN.R-project.org/package=cluster
550 Mollier A, Pellerin S. 1999. Maize root system growth and development as influenced by
551 phosphorus deficiency. J Exp Bot. 50(333):487–497. https://doi.org/10.1093/jxb/50.333.487
552 Morris GP et al. 2013. Population genomic and genome-wide association studies of agroclimatic
553 traits in sorghum. Proc National Acad Sci. 110(2):453–458.
554 https://doi.org/10.1073/pnas.1215985110
555 Niu YF et al. 2013. Responses of root architecture development to low phosphorus availability:
556 a review. Ann Bot. 112(2):391–408. https://doi.org/10.1093/aob/mcs285
557 Paradis E, Claude J, Strimmer K. 2004. APE: Analyses of Phylogenetics and Evolution in R
558 language. Bioinformatics. 20(2):289–290. https://doi.org/10.1093/bioinformatics/btg412
559 Parra-Londono S et al. 2018. Sorghum root-system classification in contrasting P environments
560 reveals three main rooting types and root-architecture-related marker–trait associations. Ann
561 Bot. 121(2):267–280. https://doi.org/10.1093/aob/mcx157
562 Peterson BG. 2020. PerformanceAnalytics: Econometric Tools for Performance and Risk
563 Analysis. R package version 2.0.4. https://CRAN.R-project.org/package=PerformanceAnalytics
564 Phillips DL et al. 2000. Minirhizotron installation in sandy, rocky soils with minimal soil
565 disturbance. Soil Sci Soc Am J. 64(2):761–764. https://doi.org/10.2136/sssaj2000.642761x
566 Rampey RA et al. 2006. An Arabidopsis Basic Helix-Loop-Helix Leucine Zipper Protein
567 Modulates Metal Homeostasis and Auxin Conjugate Responsiveness. Genetics. 174(4):1841–
568 1857. https://doi.org/10.1534/genetics.106.061044

569 Seethepalli A et al. 2020. RhizoVision Crown: An Integrated Hardware and Software Platform
570 for Root Crown Phenotyping. Plant Phenomics. 2020:3074916.
571 https://doi.org/10.34133/2020/3074916
572 Segura V et al. 2012. An efficient multi-locus mixed-model approach for genome-wide
573 association studies in structured populations. Nat Genet. 44(7):825–830.
574 https://doi.org/10.1038/ng.2314
575 Sheahan M, Barrett CB. 2017. Ten striking facts about agricultural input use in Sub-Saharan
576 Africa. Food Polic. 67:12–25. https://doi.org/10.1016/j.foodpol.2016.09.010
577 Shimizu A, Yanagihara S, Kawasaki S, Ikehashi H. 2004. Phosphorus deficiency-induced root
578 elongation and its QTL in rice (Oryza sativa L.). Theor Appl Genet. 109(7):1361–1368.
579 https://doi.org/10.1007/s00122-004-1751-4
580 Sitaraman J, Bui M, Liu Z. 2008. LEUNIG_HOMOLOG and LEUNIG Perform Partially
581 Redundant Functions during Arabidopsis Embryo and Floral Development. Plant Physiol.
582 147(2):672–681. https://doi.org/10.1104/pp.108.115923
583 Strock CF, Riva LM de la, Lynch JP. 2017. Reduction in Root Secondary Growth as a Strategy
584 for Phosphorus Acquisition. Plant Physiol. 176(1):691–703. https://doi.org/10.1104/pp.17.01583
585 Tang Y et al. 2016. GAPIT Version 2: An Enhanced Integrated Tool for Genomic Association
586 and Prediction. Plant Genome. 9(2):0. https://doi.org/10.3835/plantgenome2015.11.0120
587 Tissot N et al. 2019. Transcriptional integration of the responses to iron availability in
588 Arabidopsis by the bHLH factor ILR3. N Phytol. 223(3):1433–1446.
589 https://doi.org/10.1111/nph.15753
590 Trouche G et al. 2014. Exploring the variability of a photoperiod-insensitive sorghum genetic
591 panel for stem composition and related traits in temperate environments. Field Crop Res.
592 166:72–81. https://doi.org/10.1016/j.fcr.2014.06.008
593 Villanueva RAM, Chen ZJ. 2019. ggplot2: Elegant Graphics for Data Analysis (2nd ed.). Meas
594 Interdiscip Res Perspectives. 17(3):160–167. https://doi.org/10.1080/15366367.2019.1565254

595 Wei T, Simko V. 2021. corrplot: Visualization of a Correlation Matrix. R package version 0.92.
596 https://CRAN.R-project.org/package=corrplot
597 White PJ, Brown PH. 2010. Plant nutrition for sustainable development and global health. Ann
598 Bot. 105(7):1073–1080. https://doi.org/10.1093/aob/mcq085
599 Wissuwa M. 2003. How Do Plants Achieve Tolerance to Phosphorus Deficiency? Small Causes
600 with Big Effects. Plant Physiol. 133(4):1947–1958. https://doi.org/10.1104/pp.103.029306
601 Yi K et al. 2005. OsPTF1, a Novel Transcription Factor Involved in Tolerance to Phosphate
602 Starvation in Rice. Plant Physiol. 138(4):2087–2096. https://doi.org/10.1104/pp.105.063115
603 York LM. 2018. Phenotyping Crop Root Crowns: General Guidance and Specific Protocols for
604 Maize, Wheat, and Soybean. Methods Mol Biol (Clifton, NJ). 1761:23–32.
605 https://doi.org/10.1007/978-1-4939-7747-5_2
606